Okulov, I.V.; Boenisch, M.; Volegov, A.S.; Shakur Shahabi, H.; Wendrock, H.; Gemming, T.; Eckert, J.:

Micro-to-nano-scale deformation mechanism of a Ti-based dendritic-ultrafine eutectic alloy exhibiting large tensile ductility

In: Materials Science and Engineering A (2016) Elsevier

DOI: 10.1016/j.msea.2016.11.082

Micro-to-nano-scale deformation mechanism of a Ti-based dendritic-ultrafine eutectic alloy exhibiting large tensile ductility

I. V. Okulov[a,b,c*], M. Bönisch[a,c], A. S. Volegov[a,d], H. Shakur Shahabi[a,b], H. Wendrock[a], T. Gemming[a] and J. Eckert[f,g]

[a]IFW Dresden, Helmholtzstraße 20, D-01069 Dresden, Germany

[b]TU Dresden, Institut für Werkstoffwissenschaft, D-01062 Dresden, Germany

[c]Institute of Materials Research, Materials Mechanics, Helmholtz-Zentrum Geesthacht, Geesthacht, Germany

[d]TU Dresden, Institut für Strukturphysik, D-01062 Dresden, Germany

[e]Institute of Natural Sciences, Ural Federal University, 620000 Ekaterinburg, Russia

[f]Erich Schmid Institute of Materials Science, Austrian Academy of Sciences (ÖAW), Jahnstraße 12, A-8700 Leoben, Austria

[g]Department Materials Physics, Montanuniversität Leoben, Jahnstraße 12, A-8700 Leoben, Austria

[*]Corresponding author E-mail: okulovilya@yandex.ru

Abstract

Deformation mechanism of a new Ti-16.6Nb-6Co-5.1Cu-6.5Al (at.%) alloy is studied using scanning and transmission electron microscopy. The alloy consists of micrometer-sized β-Ti dendrites and an ultrafine-eutectic composed of β-Ti and TiCo phases. The yield strength of the alloy (1.1 GPa) is comparable to that of the metallic glass composites and is coupled with large tensile ductility of about 11 %. Transmission electron microscopy analysis reveals that slip lines formed during deformation in the dendrites penetrates the eutectic resulting in formation of a stepped interface and an extra area serving to accommodate shear strains. The β-Ti eutectic component can deform plastically to a high degree supporting deformation of TiCo. The results suggest that microstructural design of the eutectic is important for controlling tensile ductility of dendritic-ultrafine eutectic alloys.

Keywords: titanium alloy; TiCo intermetallic; ultrafine eutectic; fracture behavior; deformation mechanism; plasticity.

Introduction

As the grain size of a metallic material drops to a nano- or ultrafine size it becomes several times stronger compared to its coarse-grained state [1–10]. This exciting phenomenon

goes along a significant plasticity reduction for nano/ultrafine-grained materials [1,5,7]. One promising strategy to combine both high strength and reasonable plasticity in a metallic material is to create a bi-modal microstructure combining the high strength of a nano/ultrafine-grained structure with the good plasticity of a coarse-grained structure [11]. Examples demonstrating the effectiveness of this strategy are single-phase bi-modal copper [12] and *in-situ* formed dendrite phase-reinforced nano/ultrafine-grained eutectic alloys [13–24]. In particular, the dendritic-eutectic alloys exhibit typically plastic strains larger than 15 % and fracture stresses higher than 2 GPa [20,25–28]. The enhanced plastic deformability of the dendritic-eutectic alloys is due to the dendritic crystals which control the plastic instability of shear localization in the nano/ultrafine-grained eutectic [25,29–31]. The dendrites serve as obstacles for shear bands preventing the shearing-off through the whole sample. A similar phenomenon is also observed in metallic glass composites [32–34], where a crystalline phase controls the formation of shear band patterns and, therefore, enhances the plasticity.

There are a number of published studies investigating the compressive microdeformation mechanism of the Ti-based dendritic-eutectic alloys using transmission electron microscopy (TEM) [25,29,30,35,36]. In particular, some effort was focused on shear band formation upon compressive deformation. For example, it has been revealed that primary shear bands initiate from the interfaces between the dendrites and nano/ultrafine-grained eutectic [30]. These shear bands penetrate the interfaces mainly contributing to the overall ductility of the dendritic-eutectic alloys. Due to the typical tensile-compressive strength asymmetry [17,37] the development of Ti-based dendritic-eutectic alloys exhibiting tensile ductility [13,15,16,18,38] was postponed by several years since their discovery [31]. The tensile

strain achievable for the recently developed Ti-based dendrite-eutectic alloys reaches 12 %, e.g. for Ti-13.6Nb-6Co-5.1Cu-6.5Al (at %) [15]. The *in-situ* analysis of the microstructural evolution upon tensile loading of Ti-13.6Nb-6Co-5.1Cu-6.5Al revealed a transfer of slip bands from the dendrites into the eutectic structure [15]. It has been suggested that his slip band transfer is partially responsible for the significant tensile ductility of the Ti-13.6Nb-6Co-5.1Cu-6.5Al alloy. However, no previous studies have investigated the tensile deformation mechanism of the Ti-based dendritic-eutectic alloys using TEM.

This paper attempts to reveal the microscopic tensile deformation mechanism of the Ti-based dendritic-eutectic alloys using scanning and transmission electron microscopy. The focus is on the deformation of the ultrafine-grained eutectic and its role in enhancing the ductility of the dendritic-eutectic alloys. For this purpose, a new Ti-16.6Nb-6Co-5.1Cu-6.5Al (at %) alloy exhibiting significant tensile ductility was developed using the principles of microstructural adjustment that have been developed to improve the tensile ductility of Ti-based dendritic-eutectic alloys [13,15–18,20].

Materials and methods

The detailed experimental procedure used for casting of the samples was described in previous reports [14,15]. Structural investigation of the samples was performed by X-ray diffractometry (XRD) (STOE STADIP) with Cu-Kα_1 radiation. The X'Pert High Score Plus software was used to determine the lattice parameters from the measured patterns. Scanning electron microscopy (SEM) (Zeiss Leo Gemini 1530) coupled with energy-dispersive X-ray analysis (EDX) (Bruker Xflash 4010) was used to investigate the microstructure before and after tensile deformation. The volume fractions of the phases were analyzed by the ImageJ image analysis program. Detailed microstructural investigation of deformed samples was performed by TEM (FEI TECNAI 20, operated at 200 kV) coupled with EDX (Oxford Instruments). The TEM specimens were cut and thinned by the focused ion beam lift-out technique in a FEI HELIOS NanoLab 600i. Flat tensile test samples with 8 mm gauge length and 1 mm thickness were tested at room temperature using an Instron 8562 testing machine at an initial strain rate of 10^{-4} s^{-1}. The strain was measured by a laser extensometer (Fiedler Optoelektronik). The hardness of the individual phases was measured using an “Asmec UNAT” nano-indentor (ASMEC GmbH, Radeberg, Germany) with a cube corner tip. In order to have the indentations within the sub-micron sized single phase, a maximum load of 1 mN was selected. More than 170 indentations with a spatial distance of 4 micron were performed on a highly polished surface. The indents which were placed on a single phase were chosen based on SEM observation and corresponding load-displacement curves were treated to extract the harness values.

Results and discussions

Microstructure

XRD analysis (Fig. 1 a) reveals two phases, i.e. β-Ti (space group: *Im-3m*) and B2 TiCo (space group: *Pm-3m*), comprising the microstructure of Ti-16.6Nb-6Co-5.1Cu-6.5Al. The same phases were also reported for the parent Ti-13.6Nb-6Co-5.1Cu-6.5Al alloy [15]. The lattice parameter of β-Ti is a_0 = 0.3240 ± 0.0001 nm and of TiCo a_0 = 0.3051 ± 0.0001 nm. These values are slightly higher compared to the parent alloy what is probably due to a higher concentration of Nb in Ti-16.6Nb-6Co-5.1Cu-6.5Al. Nb exhibits a larger atomic size compared to Ti and forms a substitutional solid solution with Ti.

Figures 1 b and c shows the microstructure of the as-cast Ti-16.6Nb-6Co-5.1Cu-6.5Al alloy. Bright micrometer-sized dendrites are surrounded by an ultrafine-grained eutectic. The fraction of the dendrites was estimated to be 90-95 vol. %. According to EDX-mappings (not shown here), which reveal a very similar elemental distributions in the parent alloy [15], the dendrites are enriched in Nb and Al whereas the ultrafine-grained eutectic is enriched in Co and Cu. The SEM and XRD analyses indicate that the dendritic phase is a single β-Ti phase and the ultrafine-grained eutectic is composed of B2 TiCo and β-Ti phases. The eutectic phases, i.e. B2 TiCo and β-Ti, are arranged in lamellae with a spacing of 200 ± 50 nm, which is slightly coarser compared to the parent alloy [15]. Thus, the increase of the Nb content by 3 at% in the studied alloy has only a minor effect on the microstructure compared to the parent Ti-13.6Nb-6Co-5.1Cu-6.5Al alloy.

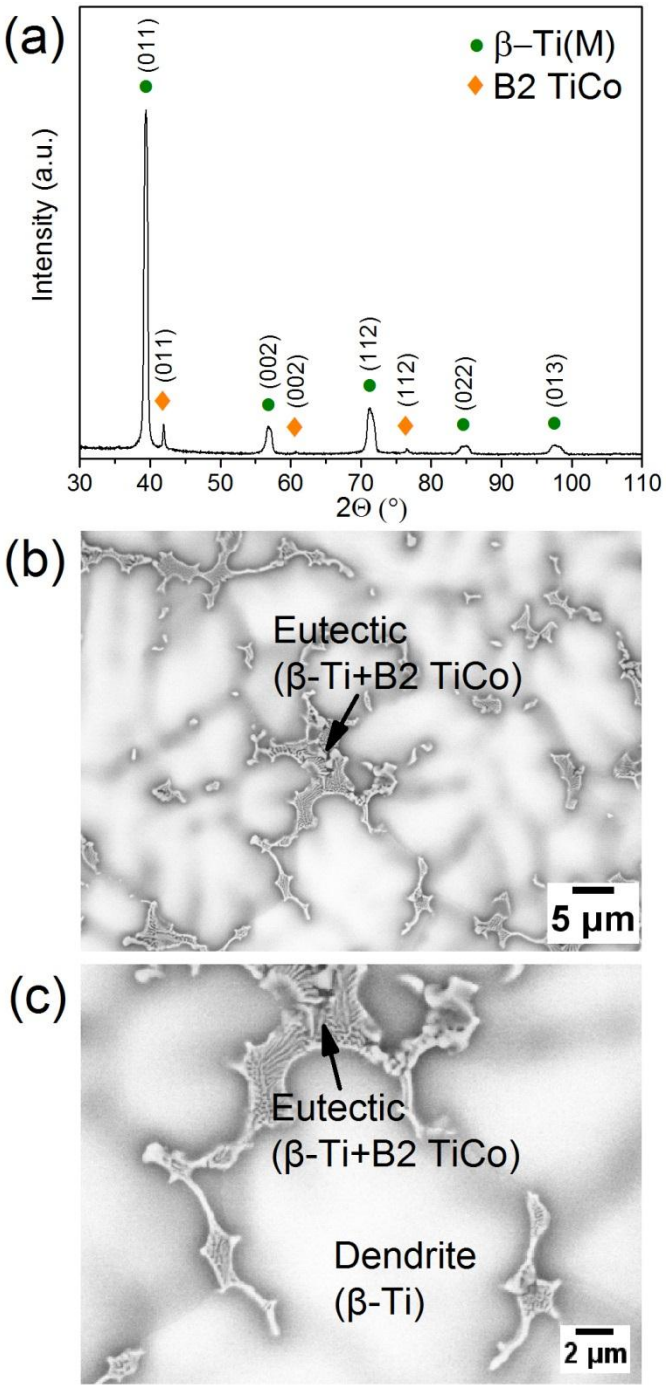

Fig. 1 *XRD pattern and SEM backscattered electron images (BSE) of the Ti-16.6Nb-6Co-5.1Cu-6.5Al (at%) alloy.*

Mechanical properties and application perspectives

A typical tensile stress-strain curve of Ti-16.6Nb-6Co-5.1Cu-6.5Al up to failure is presented in Fig. 2 a. The mechanical properties are as follows: Young's modulus E = 90.0 ± 0.5 GPa, yield strength $\sigma_{0.2}$ = 1120 ± 50 MPa, ultimate strength σ_{UTS} = 1230 ± 50 MPa, and fracture strain ε_f= 11 ± 1 % with a pronounced strain-hardening behavior. These strength characteristics of Ti-16.6Nb-6Co-5.1Cu-6.5Al are comparable with some of the recently developed Ti- and Zr-based metallic glass composites [32,39]. It is noteworthy that the fracture strain of Ti-16.6Nb-6Co-5.1Cu-6.5Al exceeds the values of many Ti-based metallic glass composites [15,39,40].

The representative nanoidentation load-displacement (P–h) curves shown in Fig. 2 a indicate that the ultrafine-grained eutectic is stronger compared to the dendritic phase. The hardness values are 5.4 GPa and 12.0 GPa for the dendrites and eutectic, respectively. Therefore, the eutectic has a larger contribution to the strength of the Ti-16.6Nb-6Co-5.1Cu-6.5Al alloy. A higher hardness of the eutectic compared to the dendrites was also reported for other Ti-based dendritic-eutectic alloys [16,17].

Combination of relatively low Young's modulus, high yield strength and large tensile ductility of the studied alloy implies its attractive application perspectives. Figs. 3 c and d presents the comparison of the studied alloy with special titanium alloys, i.e. biomedical and spring ones. Since the health of repaired bone depends on applied loads, low Young's modulus of implant metallic materials should be close to that of bone to avoid stress shielding effect [41]. On the other hand, strength of the implant material should be high enough to avoid catastrophic failure of the implant. Therefore, the metallic biomaterials can be selected based on their ratio

of yield strength-to-Young's modulus also known as mechanical bioperformance [41–43]. Fig. 3 c shows that bioperformance of the studied alloy is among the largest for bioapplicable titanium alloys. Another possible application example of the studied alloy is depicted in Fig. 3 d summarizing the data of the commercial Ti-based alloys currently used as spring materials [44–46]. High modulus of resilience is essential to consider material for spring application. The developed alloy exhibits on of the largest modulus of resilience among the selected titanium alloys (Fig. 3 d). Thus, the Ti-16.6Nb-6Co-5.1Cu-6.5Al alloy exhibits a high application potential as biomedical and spring material.

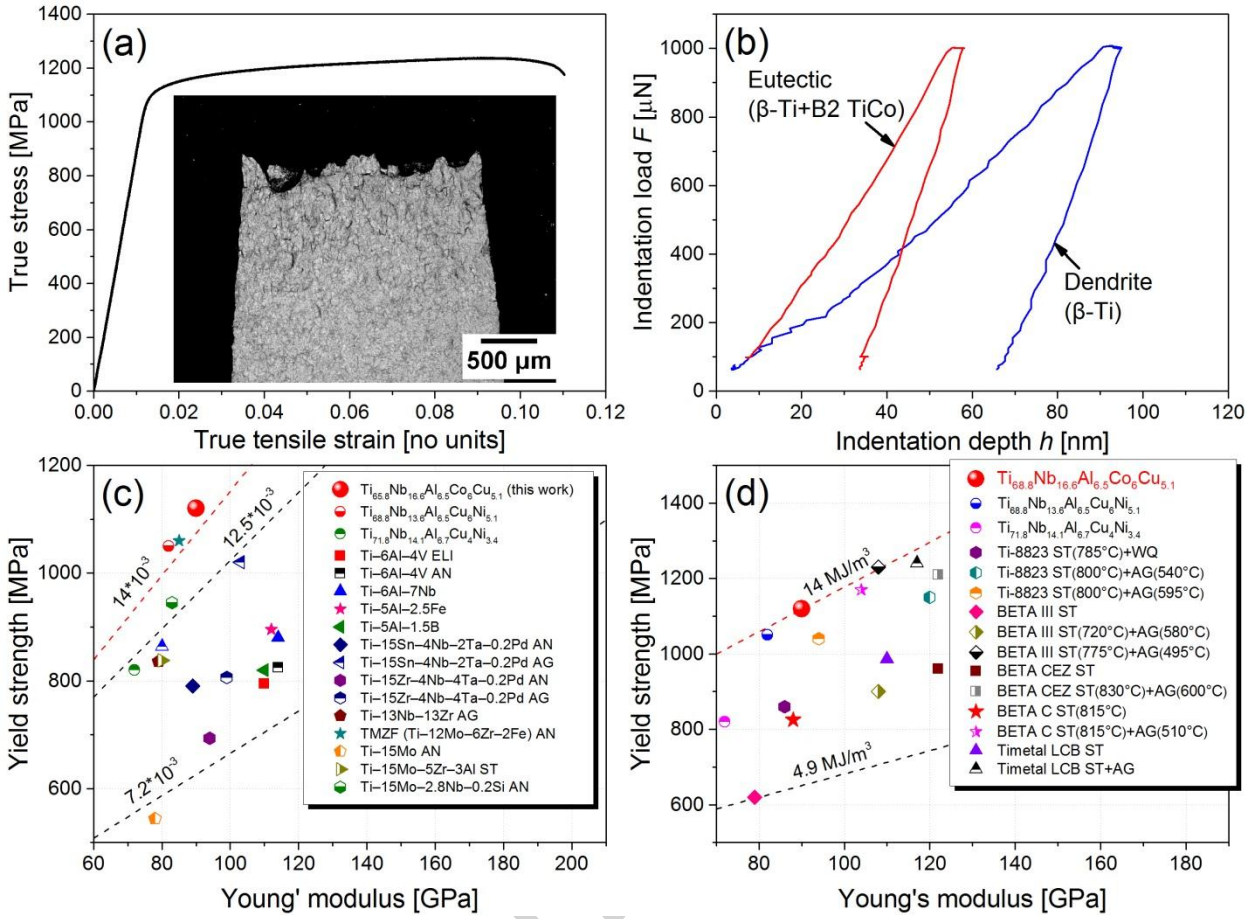

Fig. 2 *(a) True tensile stress-strain curve of the Ti-16.6Nb-6Co-5.1Cu-6.5Al (at%) alloy at room temperature (inset: sample surface after tensile fracture revealing necking); (b) Load-displacement (P-h) nanoindentation curves; (c) Yield strength plotted against Young's modulus for commercial biomedical titanium alloys* [47] *and the studied alloy of this work (Note: the dashed contours show the bioperformance $\sigma_{0.2}/E$; AN – annealed, AG – aged, ST – solution treated); (d) Yield strength plotted against Young's modulus for commercial biomedical titanium alloysused as spring materials and studied alloys (Note: the dashed contours show the resilience $(\sigma_{0.2})^2/E$; AG – aged, ST – solution treated, WQ – water quenched).*

Micro-to-nano-scale deformation mechanism

The inset in figure 2 a shows a SEM secondary electron image from the surface of the tested sample. Pronounced necking close to the fracture surface is visible and indicates that fracture occurred due to strain localization. Figures 3 a-c reveal a high density of deformation bands within the dendrites. There is no preferred orientation of these bands indicating an overall homogeneous deformation. Since strain-hardening of the studied alloy is apparent from the stress-strain curve (Fig. 2 a), these bands are slip bands formed due to dislocation movement in the dendrites. In addition, some deformation or shear bands penetrating the dendrite/eutectic interface are observed, as marked by arrows in Fig. 3 b. The transfer of the deformation bands through the dendrite/eutectic interface upon tensile loading was also observed for the Ti-13.6Nb-6Co-5.1Cu-6.5Al alloy [15] and was correlated with the cube-on-cube orientation relationship between the dendrites and the adjacent ultrafine-grained eutectic colonies. It seems that the formation of these interfacial deformation bands (or shear bands) helps to release the accumulated local strains and prevent intensive cracking of the ultrafine-grained eutectic. However, since the ultrafine-grained eutectic is intrinsically brittle, cracking of some eutectic colonies indeed takes place (Fig. 3 c). The cracks form along the dendrite/eutectic interface as well as within the ultrafine-grained eutectic. In conformity with the high plastic deformation of the studied alloy, the fracture surface reveals a ductile character (Figs. 3 f). This consists of fine micrometer-sized dimples and a few cracks. The numerous dimples result from ductile rupture of the dendrites whereas the cracks are probably due to brittle rupture of the eutectic component.

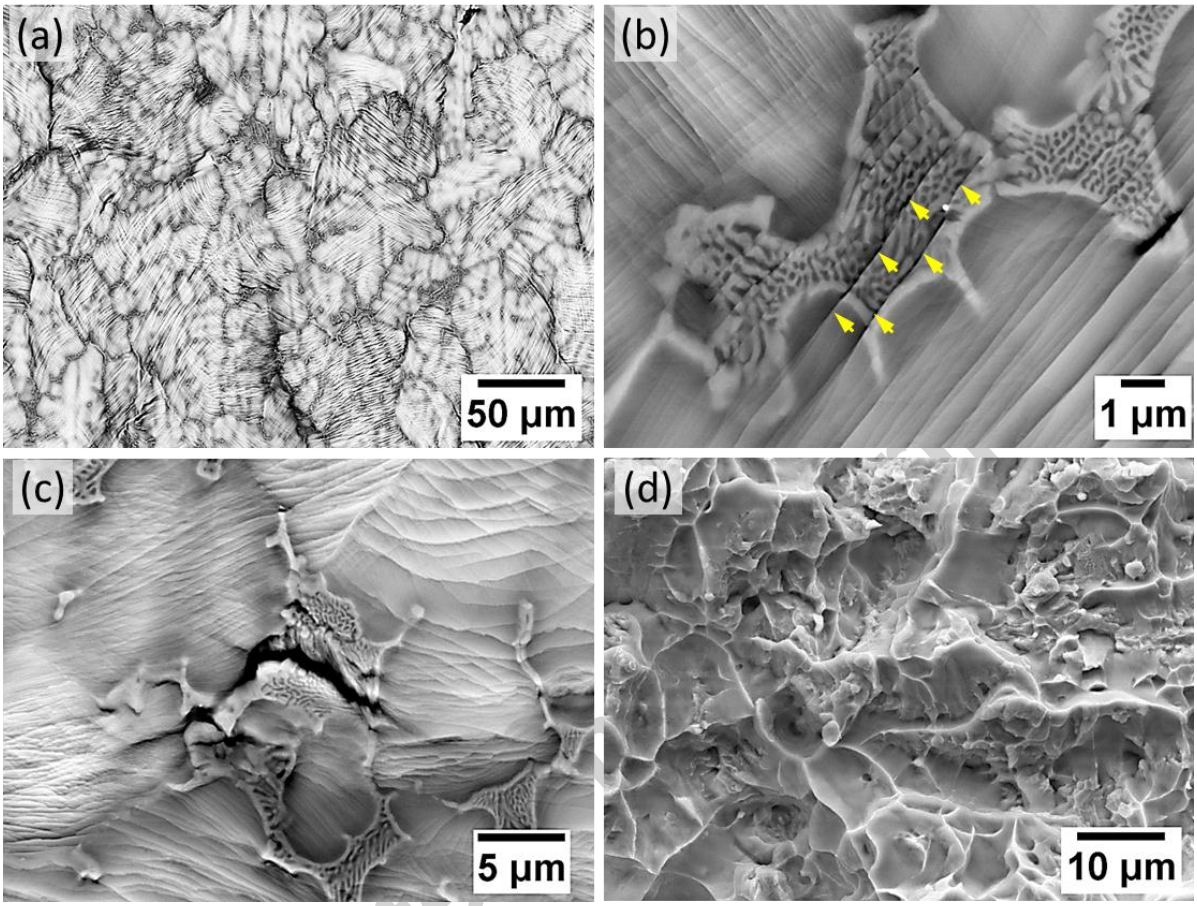

Fig. 3 *SEM micrographs of the Ti-16.6Nb-6Co-5.1Cu-6.5Al (at%) alloy after tensile fracture. (a) Morphology of the sample surface; (b) details of the* ultrafine-grained *eutectic region revealing the deformation band transmission through the dendrite/eutectic interface (shear bands are marked by arrows); (c) details of the* ultrafine-grained *eutectic region revealing the crack formation into the* ultrafine-grained *eutectic; and (d) details of the fracture surface revealing dimple fracture.*

Figure 4 presents TEM images of the Ti-16.6Nb-6Co-5.1Cu-6.5Al alloy deformed in tension to 11 %. A bcc dendrite adjacent to an ultrafine-grained eutectic zone is shown in Figure 4 a.

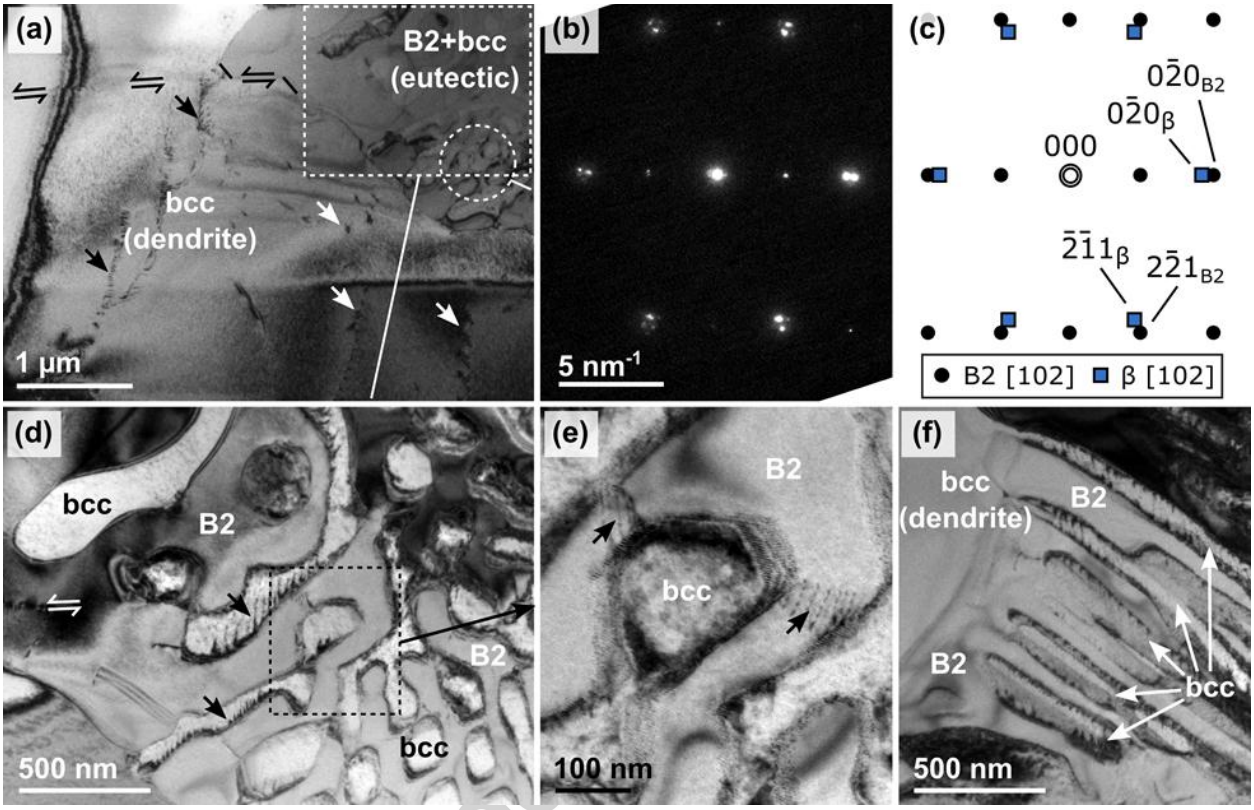

Fig. 4 *(a) Bright-field (BF) TEM image of a dendrite and the surrounding eutectic bearing signs of plastic deformation. Besides numerous dislocations (some of them are indicated by arrows) a slip line can be seen. The slip line present in the upper left corner (marked by black arrows of opposite directions) extends into the eutectic in the upper right corner. The step at the dendrite/eutectic interface is indicated by two parallel black solid lines. (b) Selected area electron diffraction pattern of the eutectic and (c) its schematic representation demonstrating the cube-on-cube orientation relationship of the eutectic components. (d) BF-TEM image of the deformed eutectic. The slip line is marked by two parallel white arrows of opposite directions. The bcc regions in the zone ahead of the slip line contain a large number of glide steps (some of them are indicated by arrows). (e) BF-TEM close-up image of the eutectic region marked in (d) showing dislocations in the B2 component. (f) BF-TEM image of heavily deformed bcc lamellae between intact B2 lamellae.*

The bcc and B2 phases in the ultrafine-grained eutectic exhibit a cube-on-cube orientation relationship, i.e. ⟨100⟩β//⟨100⟩B2, as demonstrated by the selected area electron diffraction pattern and its schematic representation in Fig. 4 b and Fig. 4 c, respectively. The same crystallographic orientation relationship for the eutectic was found in the previous study for the Ti-13.6Nb-6Co-5.1Cu-6.5Al alloy [15]. The dendrite and the ultrafine-grained eutectic appearing in Fig. 4 a did not display a particular orientation relationship but a random relative orientation.

Tensile deformation to 11 % causes the dendritic matrix to accumulate dislocations which are also visible in the dendrite shown in Fig. 4 a. The SEM investigations presented above (Figs. 3 a and b) demonstrated that plastic deformation in the present alloy occurs by glide and the formation of slip lines. The softer β-Ti dendrites yield first relative to the harder ultrafine-grained eutectic, yet at high enough stresses the slip lines are able to penetrate into the eutectic (Fig. 3 b). Such a scenario is encountered in the sample shown in Fig. 4. The dendrite (Fig. 4 a) contains a slip line which caused shearing of the ultrafine-grained eutectic. The resulting step on the interface between the ultrafine-grained eutectic and the dendrite is about 500 nm long. The formation of the stepped interface between the dendrites and the eutectic was also reported for compressively deformed Ti-8Cu-4.8Ni-7.2Sn-13.9Nb (at%)[35] and Ti-14Cu-12Ni-4Sn-10Nb (at%) [29] alloys. It was suggested that the extra area forming due to the stepped interface serves to accommodate the shear strains.

In Fig. 4 d a higher magnification image of the deformed ultrafine-grained eutectic is presented. Many defects are found along the slip line as well as close to it, in particular, inside both the B2 and bcc eutectic components. The bcc eutectic component in front of the slip line contains a

large amount of defects and glide steps, whereas the largest part of the B2 eutectic component remains intact and bears much fewer signs of plastic deformation. However, also in the B2 eutectic component dislocations and defects along and in front of the slip line were found, an example is shown in Fig. 4 e. The B2 region seen in Fig. 4 e is embedded in the highly faulted bcc regions along the extension of the slip line into the ultrafine-grained eutectic. While in the bcc eutectic component glide steps are observed that evidence plastic deformation (Fig. 4 d) no such steps were found in the B2 phase. Another example for this behavior is presented in Fig. 4 f, which shows intact B2 lamellae between bcc lamellae containing a high number of glide steps. From these observations we can conclude that the largest part of the plastic strain in the ultrafine-grained eutectic is accommodated by the bcc eutectic component while the B2 eutectic component deforms much less. Surprisingly though, the B2 phase may deform to relatively high degrees without fracturing as evidenced by the step at the dendrite/eutectic interface in Fig. 4 a. The reason for the observed ductility of the B2 phase may be the good plasticity of the surrounding bcc phase. The bcc phase is much softer than B2 thus it may easily adapt to changes in the shape of the B2 phase preventing the formation of voids at the B2/bcc interface. But at the same time the bcc eutectic component exerts a back pressure on the B2 phase thereby redistributing its load which results in a more homogeneous stress distribution in the ultrafine-grained eutectic that prevents strong strain localization. Indeed, Kim *et al* have shown that the sandwiched hcp α-Ti and bct Ti_2Cu structure of the eutectic in the Ti-8Cu-4.8Ni-7.2Sn-13.9Nb (at%) alloy is effective in releasing the shear strains [30]. In the current Ti-13.6Nb-6Co-5.1Cu-6.5Al alloy the higher crystallographic symmetry of the phases in the eutectic –

namely bcc β-Ti and B2 TiCo – might be more effective in releasing the shear strains compared to the latter example.

Conclusions

In summary, a new Ti-16.6Nb-6Co-5.1Cu-6.5Al (at%) dendritic-eutectic alloy exhibiting a large tensile ductility of 11 ± 1 % together with high strength of 1230 ± 50 MPa was designed and its deformation mechanism was studied. The fraction of the micrometer-sized dendrites composed of β-Ti is about 90-95 vol%. The ultrafine-grained eutectic consists of alternating β-Ti and B2 TiCo lamellae with a spacing of 200 ± 50 nm. The large volume fraction of β-Ti resulted in a relatively low Young's modulus of about 90 ± 0.5 GPa while the fine eutectic effectively strengthens the alloy. Comparison of the developed alloy with some special titanium alloys using Ashby plots suggests the new alloy exhibit a high application potential as biomedical and spring material. SEM and TEM of deformed tensile samples revealed that the β-Ti phase both in the dendrites and the eutectic deforms plastically to a high degree by dislocation movement and bears the major plastic deformation. The B2 eutectic component may deform to relatively high degrees without fracturing due to the support of the surrounding β-Ti eutectic and dendritic components.

Acknowledgments

The authors thank S. Donath, F. Ebert, M. Frey D. Bieberstein, T. Wiek and Ch. Damm for technical support. This work benefited from financial support by the European Commission within the framework of the FP7-MCITN network BioTiNet (PITN-GA-2010-264635), the EU and the Free State Saxony (contract number 100111842) within the European Centre for Emerging Materials and Processes Dresden (ECEMP) and Act 211 Government of the Russian Federation (contract number 02.A03.21.0006). Additional support through the German Science Foundation (DFG) under the Leibniz Program (grant EC 111/26-1), the European Research Council under the ERC Advanced Grant INTELHYB (grant ERC-2013-ADG-340025) is gratefully acknowledged.

References

[1] C.C. Koch, Ductility in Nanostructured and Ultra Fine-Grained Materials: Recent Evidence for Optimism, J. Metastable Nanocrystalline Mater. 18 (2003) 9–20. doi:10.4028/www.scientific.net/JMNM.18.9.

[2] C.C. Koch, Structural nanocrystalline materials: an overview, J. Mater. Sci. 42 (2007) 1403–1414. doi:10.1007/s10853-006-0609-3.

[3] E. Ma, Instabilities and ductility of nanocrystalline and ultrafine-grained metals, Scr. Mater. 49 (2003) 663–668. doi:10.1016/S1359-6462(03)00396-8.

[4] M.A. Meyers, A. Mishra, D.J. Benson, Mechanical properties of nanocrystalline materials, Prog. Mater. Sci. 51 (2006) 427–556. doi:10.1016/j.pmatsci.2005.08.003.

[5] I.A. Ovid'ko, Review on the fracture processes in nanocrystalline materials, J. Mater. Sci.

42 (2007) 1694–1708. doi:10.1007/s10853-006-0968-9.

[6] Y.M. Wang, E. Ma, Three strategies to achieve uniform tensile deformation in a nanostructured metal, Acta Mater. 52 (2004) 1699–1709. doi:10.1016/j.actamat.2003.12.022.

[7] D. Wolf, V. Yamakov, S.R. Phillpot, A. Mukherjee, H. Gleiter, Deformation of nanocrystalline materials by molecular-dynamics simulation: relationship to experiments, Acta Mater. 53 (2005) 1–40. doi:10.1016/j.actamat.2004.08.045.

[8] M. Dao, L. Lu, R. Asaro, J. Dehosson, E. Ma, Toward a quantitative understanding of mechanical behavior of nanocrystalline metals, Acta Mater. 55 (2007) 4041–4065. doi:10.1016/j.actamat.2007.01.038.

[9] T. Marr, J. Freudenberger, D. Seifert, H. Klauß, J. Romberg, I. Okulov, et al., Ti-Al Composite Wires with High Specific Strength, Metals (Basel). 1 (2011) 79–97. doi:10.3390/met1010079.

[10] W. Skrotzki, A. Eschke, J. Romberg, J. Scharnweber, T. Marr, R. Petters, et al., Processing of High Strength Light-Weight Metallic Composites, Adv. Eng. Mater. (2014) n/a–n/a. doi:10.1002/adem.201400190.

[11] S.H. Whang, Nanostructured metals and alloys: Processing, microstructure, mechanical properties and applications, Woodhead Publishing Limited, 2011.

[12] Y. Wang, M. Chen, F. Zhou, E. Ma, High tensile ductility in a nanostructured metal., Nature. 419 (2002) 912–5. doi:10.1038/nature01133.

[13] I. V. Okulov, U. Kühn, T. Marr, J. Freudenberger, L. Schultz, C.-G. Oertel, et al., Deformation and fracture behavior of composite structured Ti-Nb-Al-Co(-Ni) alloys, Appl. Phys. Lett. 104 (2014) 071905. doi:10.1063/1.4865930.

[14] I.V. Okulov, H. Wendrock, A.S. Volegov, H. Attar, U. Kühn, W. Skrotzki, et al., High strength beta titanium alloys: New design approach, Mater. Sci. Eng. A. 628 (2015) 297–302. doi:10.1016/j.msea.2015.01.073.

[15] I.V. Okulov, M. Bönisch, U. Kühn, W. Skrotzki, J. Eckert, Significant tensile ductility and toughness in an ultrafine-structured Ti68.8Nb13.6Co6Cu5.1Al6.5 bi-modal alloy, Mater. Sci. Eng. A. 615 (2014) 457–463. doi:10.1016/j.msea.2014.07.108.

[16] I.V. Okulov, U. Kühn, T. Marr, J. Freudenberger, I.V. Soldatov, L. Schultz, et al., Microstructure and mechanical properties of new composite structured Ti–V–Al–Cu–Ni alloys for spring applications, Mater. Sci. Eng. A. 603 (2014) 76–83. doi:10.1016/j.msea.2014.02.070.

[17] I.V. Okulov, U. Kühn, J. Romberg, I.V. Soldatov, J. Freudenberger, L. Schultz, et al., Mechanical behavior and tensile/compressive strength asymmetry of ultrafine structured Ti–Nb–Ni–Co–Al alloys with bi-modal grain size distribution, Mater. Des. 62 (2014) 14–20. doi:10.1016/j.matdes.2014.05.007.

[18] I.V. Okulov, S. Pauly, U. Kühn, P. Gargarella, T. Marr, J. Freudenberger, et al., Effect of microstructure on the mechanical properties of as-cast Ti–Nb–Al–Cu–Ni alloys for biomedical application, Mater. Sci. Eng. C. 33 (2013) 4795–4801.

doi:10.1016/j.msec.2013.07.042.

[19] I.V. Okulov, M.F. Sarmanova, A.S. Volegov, A. Okulov, U. Kühn, W. Skrotzki, et al., Effect of boron on microstructure and mechanical properties of multicomponent titanium alloys, Mater. Lett. 158 (2015) 111–114. doi:10.1016/j.matlet.2015.06.017.

[20] D. V. Louzguine-Luzgin, L. V. Louzguina-Luzgina, H. Kato, A. Inoue, Investigation of Ti–Fe–Co bulk alloys with high strength and enhanced ductility, Acta Mater. 53 (2005) 2009–2017. doi:10.1016/j.actamat.2005.01.012.

[21] J. Das, K.B. Kim, F. Baier, W. Löser, J. Eckert, High-strength Ti-base ultrafine eutectic with enhanced ductility, Appl. Phys. Lett. 87 (2005) 161907. doi:10.1063/1.2105998.

[22] G.H. Cao, R. Schneider, D. Gerthsen, R. Chulist, R. Schaarschuch, C.-G. Oertel, et al., Sn and Nb modified ultrafine Ti-based bulk alloys with high-strength and enhanced ductility, Appl. Phys. Lett. 102 (2013) 061908. doi:10.1063/1.4792592.

[23] Y.Y. Li, C. Yang, S.G. Qu, X.Q. Li, W.P. Chen, Nucleation and growth mechanism of crystalline phase for fabrication of ultrafine-grained Ti66Nb13Cu8Ni6.8Al6.2 composites by spark plasma sintering and crystallization of amorphous phase, Mater. Sci. Eng. A. 528 (2010) 486–493. doi:10.1016/j.msea.2010.09.037.

[24] D. V Louzguine-Luzgin, L. V Louzguina-Luzgina, H. Kato, A. Inoue, Investigation of high strength metastable hypereutectic ternary Ti–Fe–Co and quaternary Ti–Fe–Co–(V, Sn) alloys, J. Alloys Compd. 434-435 (2007) 32–35. doi:10.1016/j.jallcom.2006.08.335.

[25] J. Eckert, J. Das, K.B. Kim, F. Baier, W. Löser, M. Calin, et al., Deformation behavior of a

Ti66Cu8Ni4.8Sn7.2Nb14 nanostructured composite containing ductile dendrites, J. Alloys Compd. 434-435 (2007) 13–17. doi:10.1016/j.jallcom.2006.08.198.

[26] G. He, J. Eckert, W. Löser, M. Hagiwara, Composition dependence of the microstructure and the mechanical properties of nano/ultrafine-structured Ti–Cu–Ni–Sn–Nb alloys, Acta Mater. 52 (2004) 3035–3046. doi:10.1016/j.actamat.2004.03.006.

[27] G. Wang, Y.J. Huang, J. Shen, Novel TiCuNiCo composites with high fracture strength and plasticity, Mater. Des. 33 (2012) 226–230. doi:10.1016/j.matdes.2011.07.032.

[28] L.-C. Zhang, H.-B. Lu, C. Mickel, J. Eckert, Ductile ultrafine-grained Ti-based alloys with high yield strength, Appl. Phys. Lett. 91 (2007) 051906. doi:10.1063/1.2766861.

[29] B.B. Sun, M.L. Sui, Y.M. Wang, G. He, J. Eckert, E. Ma, B.B. Sun - Ultrafine composite microstructure in a bulk Ti alloy for high.pdf, Acta Mater. 54 (2006) 1349.

[30] K.B. Kim, J. Das, W. Xu, Z.F. Zhang, J. Eckert, Microscopic deformation mechanism of a Ti66.1Nb13.9Ni4.8Cu8Sn7.2 nanostructure–dendrite composite, Acta Mater. 54 (2006) 3701–3711. doi:10.1016/j.actamat.2006.04.006.

[31] G. He, J. Eckert, W. Löser, L. Schultz, Novel Ti-base nanostructure-dendrite composite with enhanced plasticity., Nat. Mater. 2 (2003) 33–7. doi:10.1038/nmat792.

[32] I. V. Okulov, I. V. Soldatov, M.F. Sarmanova, I. Kaban, T. Gemming, K. Edström, et al., Flash Joule heating for ductilization of metallic glasses, Nat. Commun. 6 (2015) 7932. doi:10.1038/ncomms8932.

[33] D.C. Hofmann, J.-Y. Suh, A. Wiest, M.-L. Lind, M.D. Demetriou, W.L. Johnson, Development of tough, low-density titanium-based bulk metallic glass matrix composites with tensile ductility., Proc. Natl. Acad. Sci. U. S. A. 105 (2008) 20136–40. doi:10.1073/pnas.0809000106.

[34] C. Hays, C. Kim, W. Johnson, Microstructure controlled shear band pattern formation and enhanced plasticity of bulk metallic glasses containing in situ formed ductile phase dendrite dispersions, Phys. Rev. Lett. 84 (2000) 2901–4. http://www.ncbi.nlm.nih.gov/pubmed/11018971.

[35] K.B. Kim, J. Das, F. Baier, J. Eckert, Propagation of shear bands in Ti[sub 66.1]Cu[sub 8]Ni[sub 4.8]Sn[sub 7.2]Nb[sub 13.9] nanostructure-dendrite composite during deformation, Appl. Phys. Lett. 86 (2005) 171909. doi:10.1063/1.1920424.

[36] K.B. Kim, J. Das, F. Baier, J. Eckert, Lattice distortion⁄disordering and local amorphization in the dendrites of a Ti66.1Cu8Ni4.8Sn7.2Nb13.9 nanostructure–dendrite composite during intersection of shear bands, Appl. Phys. Lett. 86 (2005). doi:http://dx.doi.org/10.1063/1.1929080.

[37] F.F. Wu, Z.F. Zhang, A. Peker, S.X. Mao, J. Das, J. Eckert, Strength asymmetry of ductile dendrites reinforced Zr- and Ti-based composites, J. Mater. Res. 21 (2006) 2331–2336. doi:10.1557/jmr.2006.0279.

[38] I. V Okulov, A.S. Volegov, H. Attar, M. Bönisch, M. Calin, J. Eckert, Composition optimization of low modulus and high-strength TiNb-based alloys for biomedical

applications, J. Mech. Behav. Biomed. Mater. 65 (2017) 866–871. doi:10.1016/j.jmbbm.2016.10.013.

[39] D.J. Ha, C.P. Kim, S. Lee, Correlation of microstructure and tensile properties of Ti-based amorphous matrix composites modified from conventional titanium alloys, Mater. Sci. Eng. A. 558 (2012) 558–565. doi:10.1016/j.msea.2012.08.048.

[40] D.J. Ha, C.P. Kim, S. Lee, Tensile deformation behavior of two Ti-based amorphous matrix composites containing ductile β dendrites, Mater. Sci. Eng. A. 552 (2012) 404–409. doi:10.1016/j.msea.2012.05.061.

[41] M. Geetha, A.K. Singh, R. Asokamani, A.K. Gogia, Ti based biomaterials, the ultimate choice for orthopaedic implants – A review, Prog. Mater. Sci. 54 (2009) 397–425. doi:10.1016/j.pmatsci.2008.06.004.

[42] S. Guo, Z. Bao, Q. Meng, L. Hu, X. Zhao, A Novel Metastable Ti-25Nb-2Mo-4Sn Alloy with High Strength and Low Young's Modulus, Metall. Mater. Trans. A. 43 (2012) 3447–3451. doi:10.1007/s11661-012-1324-0.

[43] K.G. Prashanth, K. Zhuravleva, I. Okulov, M. Calin, J. Eckert, A. Gebert, Mechanical and Corrosion Behavior of New Generation Ti-45Nb Porous Alloys Implant Devices, Technologies. 4 (2016) 33. doi:10.3390/technologies4040033.

[44] C. Leyens, M. Peters, Titanium and Titanium Alloys, WILEY-VCH Verlag GmbH & Co. KGaA, Weinheim, 2003.

[45] A.A. Ilyin, B.A. Kolachev, I.S. Polkin, Titanium Alloys. Composition, Structure, Properties.

Reference book., VILS-MATI, Moscow, 2009.

[46] R. Boyer, G. Welsch, E.W. Collings, Materials Properties Handbook: Titanium alloys, 4th ed., ASM International, 2007.

[47] M. Niinomi, Mechanical properties of biomedical titanium alloys, Mater. Sci. Eng. A. 243 (1998) 231–236. doi:10.1016/S0921-5093(97)00806-X.